Damage identification in a benchmark bridge under a moving load using Hilbert-Huang Transform of transient vibrations

Fernando J. Tenelema[1], Rick M. Delgadillo[1], Joan R. Casas[1]
[1]Department of Civil and Environmental Engineering, Technical University of Catalonia (UPC-BarcelonaTech), Campus Nord, C1 building. Jordi Girona, 1-3, Barcelona, Spain

email: fernando-josue.tenelema@estudiant.upc.edu, rick.milton.delgadillo@upc.edu, joan.ramon.casas@upc.edu

ABSTRACT: The damage identification process through Structural Health Monitoring (SHM) field has drawn extensive attention over the last decades for its numerous applications in failure prevention and maintenance decision-making. Several research in vibration-based methods for SHM have shown that a potential structural damage can be inferred from a change in the dynamic response of the structure. The aim of this paper is to detect and locate different damage scenarios in a benchmark bridge structure under a moving load based on Hilbert-Huang Transform (HHT). The data used in this study was obtained from the TU1402 benchmark towards enhancement of the value of SHM. The benchmark model consisted of a two-span steel bridge, where six levels of damage grouped in two damage region cases were introduced. In the proposed damage detection method, the transient vibration signals coming from a moving load in the bridge, are firstly decomposed into intrinsic mode functions (IMFs) using the Variational Mode Decomposition (VMD) approach. Then, the Hilbert Transform (HT) is applied to the IMFs. Lastly, the Marginal Hilbert Spectrum (MHS) and the Instantaneous Phase Difference (IPD) were used as damage indicators by comparing the undamaged condition of the bridge with each damage scenario. Results demonstrated that the proposed damage indicators were accurate for identifying and locating damage under transient vibration loads.

KEY WORDS: Numerical Benchmark; Hilbert-Huang Transform; Variational Mode Decomposition; Marginal Hilbert Spectrum; Instantaneous Phase Difference.

1 INTRODUCTION

To the present day, most bridges have exceeded their design service life in many parts of the world, but particularly, in Europe. Many of in-service bridges, which have been deteriorated and subjected to heavier loading situations over time, are currently classified as structurally deficient. This fact makes bridges to be more vulnerable to collapse under certain circumstances such as corrosion, traffic overloading and, particularly, lack of maintenance. This results in huge renovation and replacement costs and, in the worst cases, in human losses. Therefore, bridge maintenance, inspection and monitoring are of critical importance to prevent tragic events from happening. Within this framework, the civil engineering community has been developing multiple methods for early detection and localization of structural damage in bridges [7]-4].

Based on the concept that a potential damage to any structure can be inferred from a change in its dynamic response, numerous vibration-based damage detection methods have been deeply investigated in the past decades. However, in real structures, the presence of operational and environmental variations can also alter the measured dynamic response of the system Therefore, if these two effects are not accurately removed from the vibration signals, false-positive alerts of damage can be triggered.

As is known, it is not an easy task to collect real data on bridges in its undamaged state and in later damaged conditions, and that are simultaneously influenced by operational and environmental variations. Therefore, the use of numerical models is very useful when verifying any damage detection method. In this regard, the European Cooperation in Science and Technology (COST) organization created the scientific networking project "COST Action TU1402 on Quantifying the Value of SHM" aiming to show the high value of SHM and the validation of decision-making tools based on the Value of Information (VoI). In this paper, the TU1402 numerical benchmark [1] has been selected as a reference case study to validate a vibration-based method for damage detection using Hilbert-Huang Transform (HHT), which has been shown to be an effective technique in processing nonlinear and non-stationary data signals [7]-8].

In the proposed method of damage detection, the transient vibration signals are firstly decomposed into intrinsic mode functions (IMF) using the Variational Mode Decomposition (VMD) approach [1]. Then the Hilbert Transform (HT) is applied to the IMFs to obtain their corresponding instantaneous frequency (IF) and instantaneous amplitude (IA). Lastly, the frequency peaks obtained from marginal Hilbert spectrum (MHS) and the instantaneous phase difference (IPD) are used as damage-sensitive features. The details of the method and damage features are explained in the following sections.

As previously mentioned, the proposed method was tested using the TU1402 numerical benchmark consisting of a two-span continuous steel girder bridge. Two groups of damage (GPD1 and GPD2) were considered in order to correlate the changes in the response signals with the location and magnitude of structural damage. The results shown that the proposed method can effectively detect and locate structural damage.

2 DAMAGE DETECTION METHOD

The Hilbert-Huang Transform (HHT) method for damage detection is proposed to remove the effects of traffic loads since the recorded time series of accelerations are usually non-linear and non-stationary. In this paper, the HHT technique consists of the application of variational mode decomposition (VMD) and Hilbert transform (HT). Figure 1 shows the flowchart of the proposed methodology for damage detection using the TU1402 numerical benchmark.

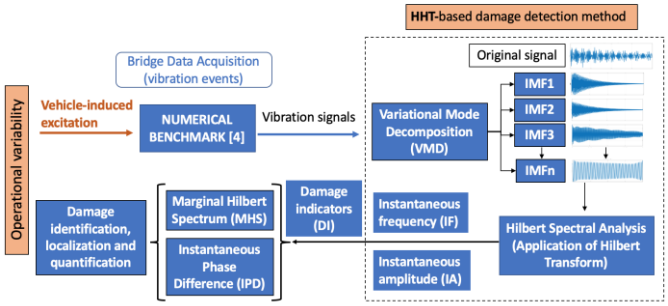

Figure 1. Proposed damage detection methodology

2.1 *Variational mode decomposition*

The first stage of the proposed HHT technique consists on the decompposion of a multicomponent signal into an ensemble of quasi-orthogonal band-limited IMF. Dragomiretskiy and Zosso [9] developed the Variational Mode Decomposition (VMD) method to overcome certain drawbacks in the EEMD method or its variations when adding white Gaussian noise to measured signals.

For this particular study case, the first author demonstrated on his master's thesis [10] that the VMD-based method presented significant advantages compared with the empirical methods, as listed below:

- mitigation of the mode mixing problem,
- lower computational cost and error,
- suitable for a high frequency range,
- and better orthogonality of IMFs.

The VMD method, which is an adaptative, non-recursive and theoretically well-founded decomposition technique, can be interpreted as a constrained variational problem. Mathematically it can be written as

$$\min_{\{u_k\},\{\omega_k\}} \left\{ \sum_k \left\| \partial_t \left[\left(\delta(t) + \frac{j}{\pi t} \right) u_k(t) \right] e^{-j\omega_k t} \right\|_2^2 \right\} \quad \text{subject to} \quad \sum_k u_k = f \tag{1}$$

It should be pointed out that before the application of VMD, several parameters must be specified, such as: the relative tolerance (ε_r), penalty factor ($\tilde{\alpha}$), fidelity coefficient (τ), number of optimization iterations (O) and the number of modes (K). According to Tenelema [10], physically meaningful IMFs can be obtained by using ε_r =1e-10, $\tilde{\alpha}$ = 500, τ = 0.1, and O =100000 for all sensors and damage scenarios, and by varying the number of modes, K, from one sensor to another depending on the predominance of the selected modes of vibration in the dynamic behavior of the structure. The value of K will be discussed in the following sections.

2.2 *Marginal Hilbert spectrum (MHS)*

The second stage of the proposed HHT technique consists of the application of Hilbert transform (HT) to the IMFs in order to find their corresponding instantaneous energy and instantaneous frequency. This results in a time-frequency-energy relationship which is usually represented by a Hilbert Spectrum (HS) contour plot, noted as $H[f_k(t), t]$. Then, the marginal Hilbert spectrum (MHS) can be obtained by integration of the HS over a particular data length, as in (2)

$$H\left[f_k(t)\right] = \int_{T_0}^{T_f} H\left[f_k(t), t\right] dt \tag{2}$$

Where T_o and T_f represent the initial and final time step chosen for spectral analysis, respectively. The MHS measures the total energy contribution from each frequency value per IMF. It has been shown by several authors [7], [8] that the MHS can be used as an indicator of damage.

2.3 *Instantaneous phase difference (IPD)*

The total instantaneous phase function at a particular point p, $\theta p(t)$, is defined as the sum of the instantaneous phases for the selected IMF $\theta k(t)$.

$$\theta(t) = \sum_k \theta_k(t) = \sum_k \arctan\left(\frac{H\left[x_k(t)\right]}{x_k(t)} \right) \tag{3}$$

Where $x_k(t)$ denotes the IMFs(t) selected for spectral analysis and $\theta p(t)$ represents the total number of rotations of the original signal in the complex plane, expressed in radians (rad) [6]. In other words, $\theta p(t)$ denotes the phase of traveling structural waves of a dynamically measurable quantity (e.g., acceleration), as highlighted by Salvino et al. [11]. Moreover, Kunwar et al. [7] mentioned that for structural damage identification purposes, the instantaneous phase must be unwrapped from its harmonic nature by representing all local oscillations in the data as a monotonically increasing function.

The instantaneous phase difference at a particular sensor p, $\varphi_p^C(t)$, is defined as the instantaneous phase of a travelling wave at sensor *p* for a given condition *C* of the bridge, $\theta_p^C(t)$, minus the instantaneous phase for the undamaged condition at a reference sensor *o*, $\theta_o^{UND}(t)$, as shown in (4).

$$\varphi_p^C(t) = \theta_p^C(t) - \theta_o^{UND}(t) \tag{4}$$

The location of the reference sensor will be discussed in the following sections. It can be also deduced that by definition any change in the dynamics of the bridge will be reflected in the IPD since the speed at which energy travels through the

structure might be altered when damage occurs. Therefore, tracking changes in the wave speed of response measurements is an effective technique for damage identification and localization.

3 CASE STUDY

3.1 Numerical benchmark

The numerical benchmark developed by Prof. Tatsis and Prof. Chatzi from ETH Zürich is studied in this paper. The benchmark represents a plane stress problem of the superstructure of a two-span continuous steel girder bridge. The bridge is represented by a FE model as shown in Figure 2, with equal span lengths of 10m, a total height of 0.6m and a thickness of b = 0.1m. Regarding the mechanical properties of the bridge, it has a linear elastic material behavior with Young's modulus E = 215 GPa, Poisson's ratio ν = 0.3 and material density ρ = 7850 kg/m3 at ambient temperature of T = 20ºC.

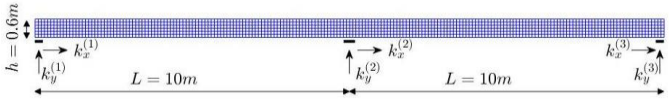

Figure 2. Two-span continuous steel girder bridge

Three identical and equally spaced elastic supports are considered: two supports acting at both ends in a width of 0.3m and one intermediate support acting in the middle of the beam in a width of 0.4m. All supports are modelled as point spring supports, each with two degrees of freedom. In order to avoid the mixing of the longitudinal and vertical bending mode shapes, the horizontal and vertical stiffness of springs are $k_x = 10^6$ kN/m and $k_y = 10^{12}$ kN/m, respectively.

A four-node bilinear isoparametric element referred as QUAD4 was implemented with full integration by using a 2×2 Gauss quadrature rule. After a mesh convergence study, a mesh element size of 0.05m × 0.05m was chosen on the basis of computational cost and accuracy in the maximum vertical displacements. As shown in Figure 2, the model is discretized in 400 and 12 elements in x and y directions, respectively, resulting in 4800 elements and 5213 nodes in total (10426 degrees of freedom).

3.2 Damage scenarios and sensors

In this case study, the structural damage is modelled as a reduction of the bridge superstructure's stiffness, more specifically, as a reduction of Young's modulus at the Gauss points on the selected damaged elements. Two damage regions are considered as shown in Figure 3; one where the damage is located in the center of the left span and the other over the intermediate elastic support, covering different numbers of damaged elements and resulting in six damage scenarios (DMG).

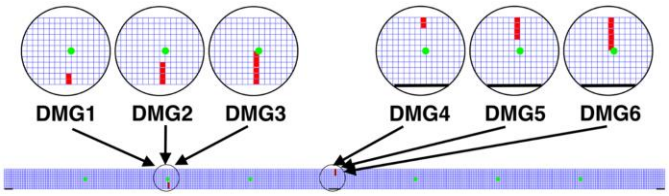

Figure 3. Damage locations (red squares) and sensors (green dots) on steel beam.

For instance, DMG1 and DMG4 cover an area of two damaged elements, DMG2 and DMG5, a zone of four damaged elements, while DMG2 and DMG6, a zone of six damaged elements. Therefore, the damage area will always have a constant width of 0.05m and a height ranging from 0.1 to 0.3m.

On the one hand, in order to study the influence of damage severity related to the percentage of stiffness reduction (SR), the Group of damage 1 (GPD1) is created. It consists of the undamaged condition of the bridge and the damage scenario 3 (DMG3) with a stiffness loss of 50%, 70% and 90%. On the other hand, in order to study the effects of damage depth related to the number of damaged elements, the Group of damage 2 (GPD2) is created. It consists of the undamaged condition of the bridge and the damage scenario 4 (DMG4), DMG5 and DMG6 with the same stiffness loss of 70%. Both groups of damage are described in the table below.

Table 1. Description of the groups of damage considered for study

Group of damage GPD	Location, x (m)	Damage scenarios, DMG	Stiffness reduction, SR (%)
GPD 1	5	UND	-
		DMG3	50
		DMG3	70
		DMG3	90
GPD 2	10	UND	-
		DMG4	70
		DMG5	70
		DMG6	70

Lastly, seven measurement points called "sensors" are considered to provide information about the displacements and accelerations over time in both horizontal (x) and vertical (y) directions. The location of these sensors are shown as green points in the Figure 3 and described in the table below:

Table 2. Location of sensing points

Sensors	Description: location along the neutral axis of the beam (y=0.3m)
S-01	x = 2.5 m
S-02	x = 5.0 m
S-03	x = 7.5 m
S-04	x = 12.5 m
S-05	x = 15.0 m
S-06	x = 17.5 m
S-07	x = 10.0 m

3.3 *Modal analysis*

A modal analysis was firstly performed to obtain the natural frequencies of the bridge and their corresponding mode shapes. As the vibration modal solutions are based on sinusoidal functions, modes can be either symmetric or asymmetric. This spatial property has an impact on the effective mass participation factor (EMPF) corresponding to each mode of vibration. The EMPF represents the quantity of the system mass participating in a particular mode for a particular direction (x or y direction). Therefore, the larger the EMPF of a particular mode, the greater the contribution of this mode to the dynamic response.

Figure 4 shows the first eight mode shapes along with their corresponding natural frequencies (in Hz) and EMPFs (in %) in the y-direction of excitation.

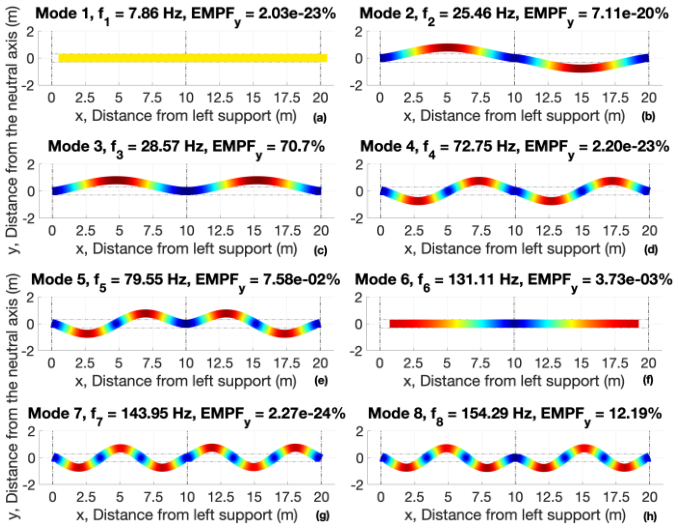

Figure 4. First eight mass-normalized mode shapes using a scaling factor of 50.

Since a vertical load is considered to simulate traffic, only the vertical bending (VB) modes are relevant to be studied. That is, modes 2, 3, 4, 5, 7, and 8 are selected, representing the first symmetric (~25Hz), first asymmetric (~29Hz), second symmetric (~73Hz), second asymmetric (~80Hz), third symmetric (~144Hz) and the third asymmetric (~154Hz) vertical bending modes (VB), respectively. Tenelema [10] demonstrated that only the first three bending modes, with their corresponding symmetric and asymmetric components, are enough to represent the dynamic behavior of the structure, having a cumulative EMPF of almost 83% and being modes 3 and 8 the first two predominant modes based on their EMPF.

3.4 *Time-history analysis*

To perform a time history analysis of the vehicle-bridge system, the implicit Newmark integration schema is considered. A detailed description of this method can be found in [12]. In this case study, the parameters used for the application of Newark's algorithm are:

- $\hat{\alpha}$ = 1/2 is set to avoid the presence of artificial damping,
- $\hat{\beta}$ = 1/6 is set to assume a linear variation of the acceleration of mass in motion between two consecutive time steps,
- Δt_c = 0.0001 seconds is set to ensure the stability of the method.

Rayleigh damping is used to compute the damping matrix. The Rayleigh coefficients, α = 0.2341 and β = 3.8769e-6 are obtained from the damping ratios specified for the first two predominant modes (ζ_3 = 0.1% and ζ_8 = 0.2%) as explained in [10].

Regarding the loading, the weight of a standard car truck of 3 tons is considered. Besides, in order to avoid the influence of the forced frequencies on the dynamic response due to the transient load, while guaranteeing enough time samples for the time history analysis a vehicle speed of v = 10m/s (36km/h) is considered.

The vertical displacements and accelerations are determined up to 2 seconds, which corresponds to how long the vehicle takes to go from one end of the bridge to the other. A sampling frequency of f_s = 400Hz is selected, resulting in a Nyquist frequency of 200Hz which is greater than the maximum natural frequency of the selected modes (f_8=154Hz). Therefore, the six bending modes previously selected will be accurately represented in the vehicle-induced vibrations.

The vertical time-history accelerations recorded by sensors 1, 2 and 7 are shown in Figure 5, Figure 6 and Figure 7, respectively, for the intact state of the bridge and the damage scenario 3 with a stiffness reduction of 90%. From these figures, it can be observed that the vibration signal is altered from the undamaged condition due to the presence of damage.

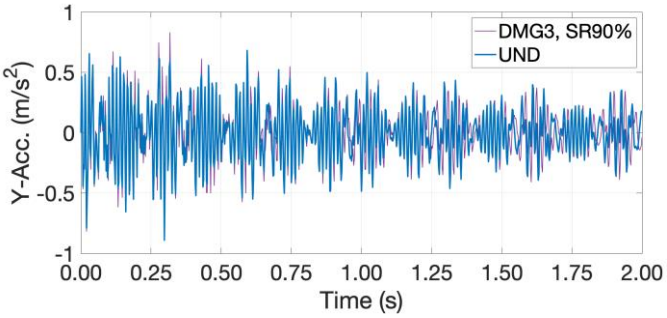

Figure 5. Vertical Accelerations – Sensor S-01.

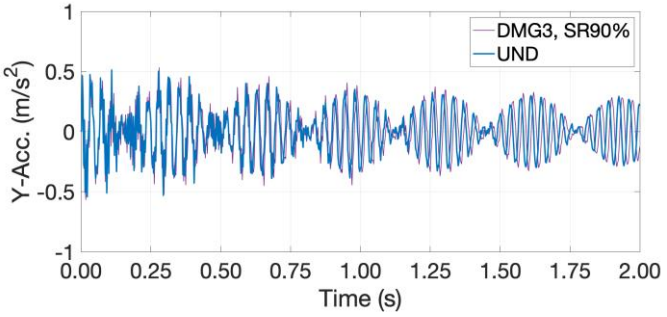

Figure 6. Vertical Accelerations – Sensor S-02.

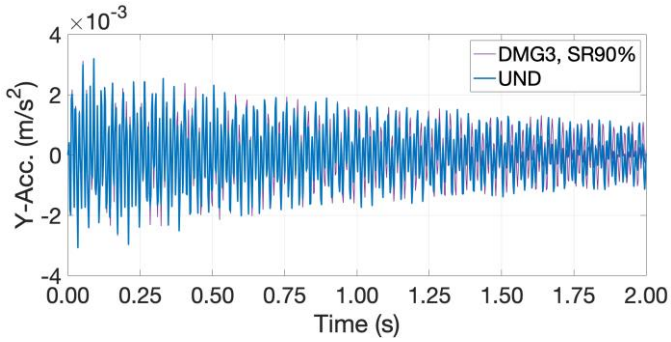

Figure 7. Vertical Accelerations – Sensor S-07.

Besides, it can be seen from the figures above that the waveform shape of the vertical accelerations differs from one sensor to another due to the contribution of the bending modes at a particular location of a sensor. In other words, for a particular bending mode, if the location of a node, which is associated to minimum amplitudes, coincides with the location of a sensor, then the contribution of this mode to the vibration signal is meaningless. This behavior can be seen from Figure 6, where the 1st and 3rd bending modes prevail over the 2nd bending mode since sensor 2 is located in a node regarding the modes 4 and 5, as seen in Figure 4. Therefore, the vertical accelerations recorded in sensors S-01, S-03, S-04 and S-06 are quite similar since all of them are located at ¼ from an elastic support, as in the case of sensors S-02 and S-05 since they are placed at the middle of each span. Lastly, sensor 7 is a particular case where only the asymmetric bending modes (modes 3, 5 and 8) largely contribute to the dynamic response of the bridge.

4 RESULTS AND DISCUSSION

4.1 Intrinsic Mode Functions using VMD

The Intrinsic Mode Functions (IMFs) obtained from the vibration signals via the Variational Mode Decomposition technique are shown in Figure 8 for sensor S-01 and S-02.

After several experiments, it has been shown that the VMD-based method is not capable to separate the asymmetric and symmetric components when their contribution to the dynamic response is minor. For this reason, the number of modes K set for the application of VMD is different for each sensor: K=6 for sensors S-01, S-03, S-04 and S-06; K=5 for S-02 and S-05; K=3 for sensor S-07.

Besides, it can be seen from Figure 8 that the mode mixing problem is mitigated and physically meaningful IMFs can be obtained. However, the boundary effects problem is the main limitation of the VMD method which can be noted at the beginning and at the end of the waveform of accelerations.

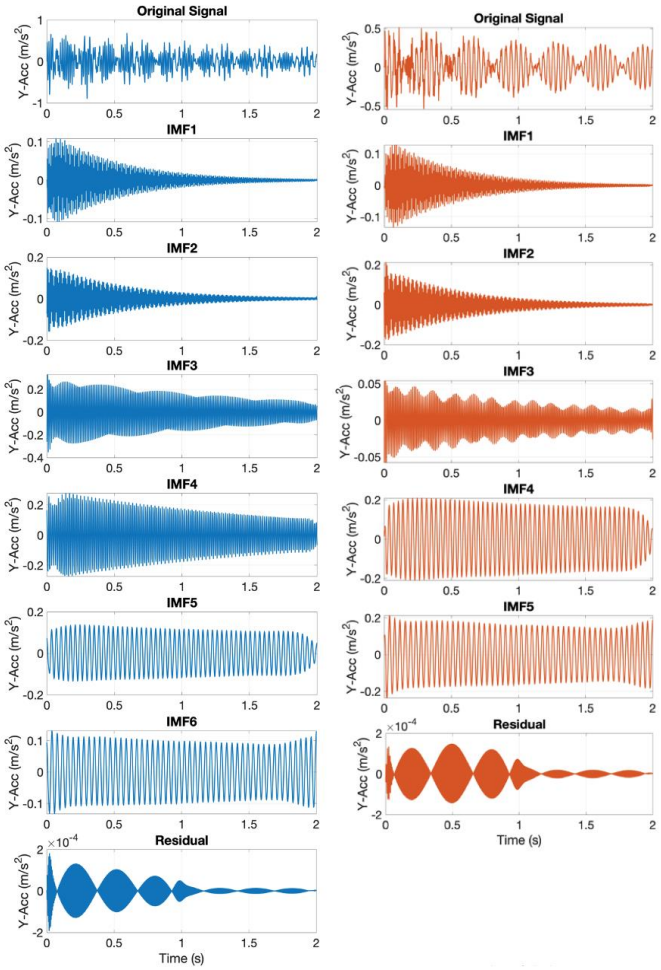

Figure 8. The IMFs obtained in sensor S-01 (left column) and S-02 (right column) using VMD.

4.2 Frequency peaks in the MHS

Firstly, to mitigate the boundary effects due to the application of Hilbert Transform, the study interval selected is $[T_o, T_f]$ = [0.05, 1.875] seconds. Figure 9 shows the marginal Hilbert spectrum (MHS) obtained in sensor S-01 corresponding to the undamaged and damage scenarios of the GPD1. Six well-differentiated regions can be identified which are associated to the six IMFs lying within their associated frequency content. From this graph, the frequency peaks corresponding to the maximum energy value can be extracted. However, it is difficult to identify clear frequency peaks in certain regions such as around 154Hz (IMF1) and 25Hz (IMF6). Hence, they are not suitable for comparison purposes. The rest of the IMFs show a better frequency distribution; hence they are studied in more detail. It can be seen that from the IMF2 to IMF5 the frequency peaks reduce when damage occurs, as expected. However, the percentage of frequency reduction is very subtle in the intermediate-frequency modes (IMF 3 and IMF4), compared to the high-frequency mode 7 (IMF2) and to the low-frequency mode 3 (IMF5).

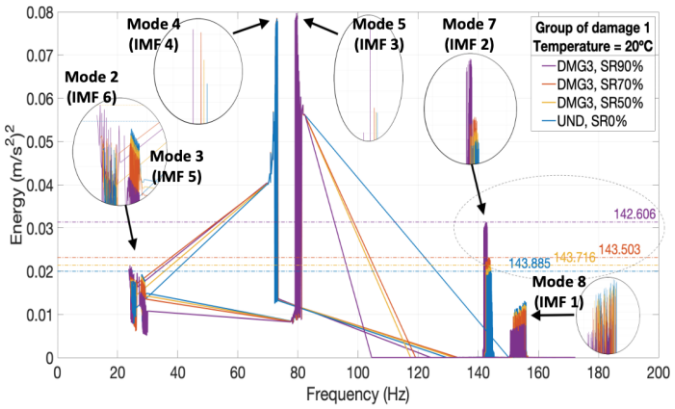

Figure 9. MHS obtained in sensor S-01 for the GPD1.

Figure 10 shows the MHS obtained in sensor S-02 corresponding to the undamaged and damage scenarios of the GPD1. On the one hand, it can be observed mode mixing in IMF3 due to the very low energy contribution of the 2nd bending mode to the dynamic response. Therefore, the frequency peaks found in modes 4 and 5 are not clear and not suitable for comparison purposes. On the other hand, it can be noted that the frequency peaks reduce when damage occurs for both the high-frequency modes (IMF1 and IMF2) and low-frequency modes (IMF4 and IMF5).

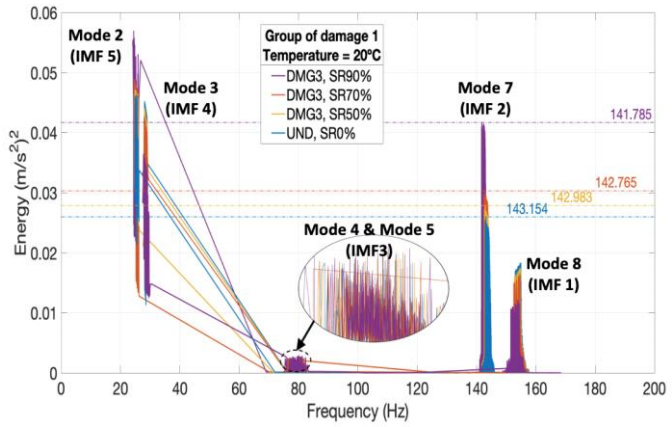

Figure 10. MHS obtained in sensor S-02 for the GPD1.

For the reasons given above, only the modes that can be compared among the sensors are the 1st asymmetric bending mode (mode 3) and the 3rd symmetric bending mode (mode 7). In this paper, the influence of high- frequency modes is considered for damage detection. Then, henceforth, all the results are referred to the 3rd symmetric bending mode (IMF2) regarding the GPD1.

Figure 11, show the MHS for each damage configuration of the GPD2 in sensor S-07. It can be observed that the predominant modes are the asymmetric 1st, 2nd and 3rd bending modes. It is also noticeable that when the depth of damage increases the peak of energy also increases, as opposed to the peak of frequency that reduces. This behavior indicates the presence of damage as noted by many authors [7-8].

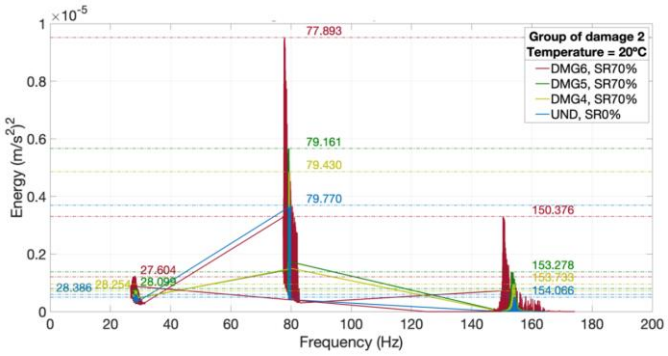

Figure 11. MHS obtained in sensor S-01 for the GPD2.

Figure 12 and Figure 13 show the MHS for each damage configuration of the GPD2 in sensors S-01 and S-02, respectively.

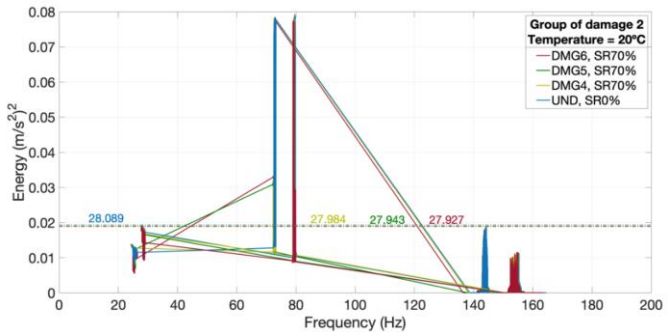

Figure 12. MHS obtained in sensor S-02 for the GPD2.

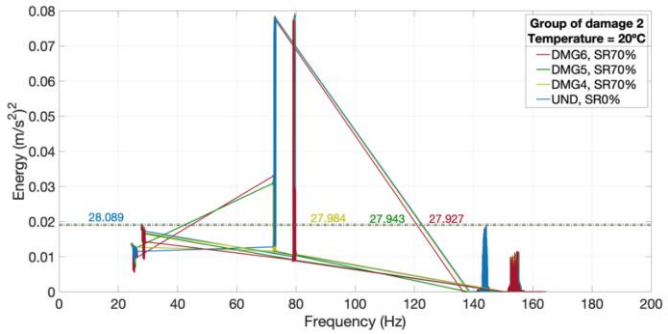

Figure 13. MHS obtained in sensor S-02 for the GPD2.

As is to be expected, for all the sensors, the peak frequency decreases as the damage depth increases. Tenelema [10] showed that for the GPD2 the frequency peaks extracted from the low-frequency asymmetric mode (mode 3) were reliable for damage detection purposes and useful to be compared among the sensors.

The results of the percentage reduction in frequency peaks for each sensor and each damage scenario of the GPD1 and GPD2 are summarized in Table 3 and Table 4, respectively. It can be seen that when the level of damage increases, the percentage reduction increases as well. For the GPD1, the largest difference in frequencies are found in sensor S-02, and for the GPD2 it is found in sensor S-07, coinciding with the damage location.

Table 3. Percentage reduction in GPD1.

Sensor	DMG3, SR50%	DMG3, SR70%	DMG3, SR90%
S-01	0.1176	0.2661	0.8968
S-02	**0.1194**	**0.2725**	**0.9653**
S-03	0.1124	0.2596	0.9295
S-04	0.0746	0.1804	0.8117
S-05	0.0745	0.1840	0.8074
S-06	0.0794	0.1969	0.8312

Table 4. Percentage reduction in GPD2

Sensor	DMG4, SR70%	DMG5, SR70%	DMG6, SR70%
S-01	0.3752	0.5235	0.5821
S-02	0.2917	0.5486	0.6507
S-03	0.2620	0.6511	0.8189
S-04	0.3311	0.2984	0.3519
S-05	0.2044	0.2615	0.3477
S-06	0.0804	0.2642	0.3744
S-07	**0.4697**	**1.0243**	**2.8360**

From this perspective, the MHS not only aids to detect and reflect the damage severity (GPD1) and damage extension (GPD2), but also to locate the structural damage based on the largest reduction of frequency peaks among the selected sensors. Therefore, the MHS is an effective parameter to detect, locate and quantify damage.

4.3 Instantaneous phase difference (IPD)

For the GPD1, in order to obtain a similar order of magnitude in the instantaneous phase difference (IPD) among the sensors by taking sensor S-06 as a reference point, only the 1st and 3rd bending modes are considered. Figure 14 illustrates the IPD for each sensor and each damage scenario. It can be observed that all sensors indicate a successful assessment of damage detection since the IPD is reduced when damage occurs reflecting the severity of damage as well. It should be pointed out that for the DMG3 with SR90%, the IPD has been enormously decreased compared to the other damage scenarios due to a high percentage of stiffness reduction.

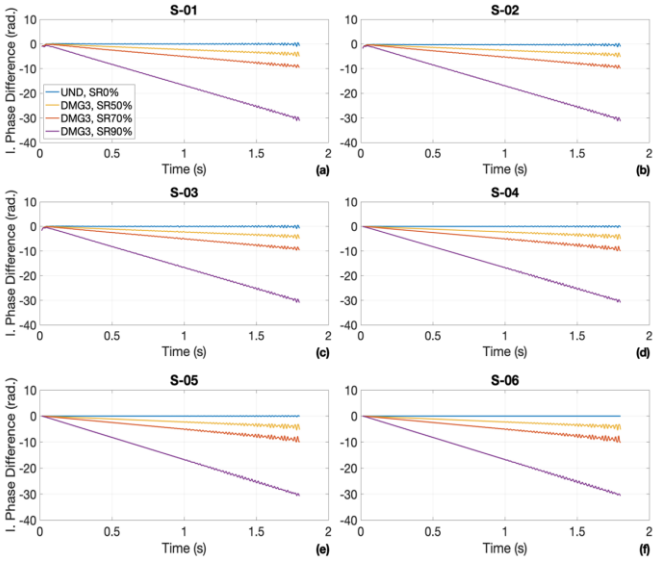

Figure 14. IPD obtained in each sensor for the GPD1.

For the GPD2, all bending modes are considered since the reference point is taken at each sensor p for the undamaged condition. Figure 15 shows the IPD for each sensor and each damage scenario of the GPD2. It can be observed that the IPD is reduced when damage occurs, and it gets further reduced when the depth of damage grows.

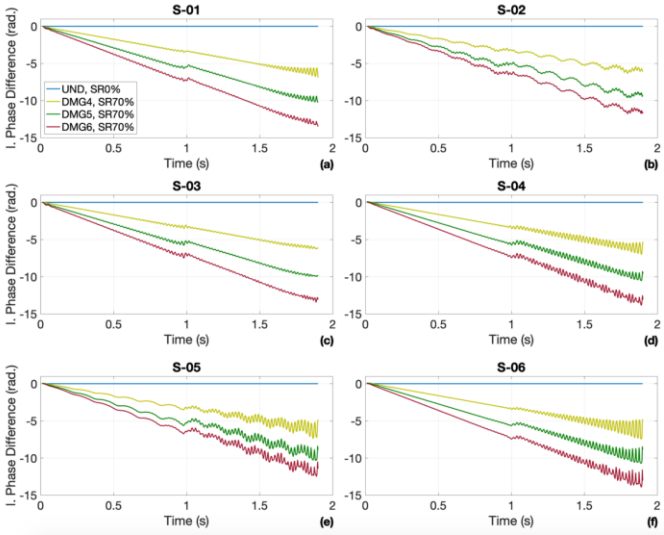

Figure 15. IPD obtained in each sensor for the GPD2.

Besides, there is a singularity in all the sensors around 1 second. At this time step, a small jump can be seen coinciding with the location of damage, thus the IPD is also good indicator for damage location. Moreover, it can be deduced that for a fixed stiffness reduction (SR) when the number of damaged elements increases, the reduction in the IPD is more proportional than when varying the SR with a fixed number of damaged elements, as seen in Figure 15.

To conclude, tracking changes in the wave speed via the instantaneous phase difference is also an effective technique for the identification, localization and quantification of damage.

5 CONCLUSIONS

In order to achieve the first three levels of SHM (damage detection, localization and quantification of damage), vertical acceleration measurements obtained from seven sensors equally spaced along the bridge-like structure were analyzed by means of the application of the Hilbert–Huang transform (HHT) based method.

Regarding the first step of HHT-based method and for this numerical benchmark, it has been shown that the EMD-based methods present some drawbacks such as a high computational cost, noise remaining in the IMFs and the inability to accurately decompose closely spaced spectral modes (asymmetric and symmetric) into different IMFs. In other words, the excessive rigidity of the bridge, resulting in high natural frequencies ranging from 25Hz to 155Hz, makes it difficult to obtain physically meaningful IMFs. On the contrary, the application of the VMD-based method ensures no mixture of modes as well as the orthogonality of the transformation, leading to reliable results in time-frequency analysis.

Regarding the second step of HHT-based method, the marginal Hilbert spectrum (MHS) and the instantaneous phase difference (IPD) are proposed as damage indicators for this bridge-like structure subjected to traffic loads. The results of these two parameters for damage detection are highly satisfactory regarding both groups of damage. As far as the MHS is concerned, the frequency peaks reduce when damage occurs due to stiffness loss in all sensors for the most significant modes. Moreover, those sensors located closer to the damage zones show a more significant percentage reduction than the sensors placed further away. Hence, damage can not only be detected, but also localized and quantified by assessing the percentage reduction of the frequency peaks extracted from the MHS. Regarding the phase difference phase (IPD), all sensors detect a reduction of the IPD when damage occurs due to a change of the speed at which the energy travels through the structure. Moreover, all sensors are capable to detect the intensity of the damage, simulated by an increase of the stiffness loss (GPD1), and the extension of the damage, simulated by an increase of the number of damaged elements. However, only in the GPD2, the IPD has been able to locate damage since singular variations of the travelling energy occur when damage is located above the mid-support.

To conclude, both the spectral peak frequency and the instantaneous phase difference have shown to be useful features to detect, locate and quantify damage in a bridge-like structure under operational loads for certain levels of damage.

ACKNOWLEDGMENTS

The second author acknowledges the financial support provided by the Government of Peru through the Educational Credit Program PRONABEC, as well as his Ph.D. Scholarship. The authors are grateful to Prof. Eleni Chatzi, ETH Zurich, Switzerland for the valuable numerical benchmark data assessed within this study. Authors are indebted to the Secretaria d' Universitats i Recerca de la Generalitat de Catalunya for the funding provided through AGAUR (2017 SGR 1481).

REFERENCES

[1] An Y, Chatzi E, Sim SH, Laflamme S, Blachowski B, Ou J. *Recent progress and future trends on damage identification methods for bridge structures*. Structural Control and Health Monitoring. 2019 Oct;26(10):e2416.

[2] Delgadillo RM, Casas JR. *Non-modal vibration-based methods for bridge damage identification*. Structure and Infrastructure Engineering. 2019 Aug 8:1-22.

[3] Entezami A, Sarmadi H, Behkamal B, Mariani S. *Big Data Analytics and Structural Health Monitoring: A Statistical Pattern Recognition-Based Approach*. Sensors 20.8 (2020): 2328.

[4] Cremona C, Santos J. *Structural health monitoring as a big-data problem*. Structural Engineering International. 2018 Jul 3;28(3):243-254.

[5] K. Tatsis and E. Chatzi, *A numerical benchmark for system identification under operational and environmental variability*, in Proceedings of the 8th International Operational Modal Analysis Conference (IOMAC 2019), Copenhagen, Denmark, 2019.

[6] N. E. Huang, K. Huang, and W.-L. Chiang, *HHT-based bridge structural health-monitoring method," in Hilbert-Huang Transform and Its Applications*, vol. 5, pp. 263–287, 2005.

[7] A. Kunwar, R. Jha, M. Whelan, and K. Janoyan, *Damage detection in an experimental bridge model using Hilbert–Huang transform of transient vibrations*, in Structural Control and Health Monitoring, vol. 20, no. 1, pp. 1-15, 2013.

[8] J. J. Moughty and J. R. Casas, *Evaluation of the Hilbert Huang transformation of transient signals for bridge condition assessment*, in Proceedings of the Annual European Safety and Reliability Conference (ESREL 2017), Portoroz, Slovenia, 2017.

[9] K. Dragomiretskiy and D. Zosso, *Variational mode decomposition*, IEEE transactions on signal processing, vol. 62, no. 3, pp. 531-544, 2013.

[10] F. J. Tenelema, *Bridge Damage Identification under operational and environmental variability*, Master's thesis, Barcelona, Spain, 2020.

[11] L. W. Salvino, D. J. Pines, M. Todd, and J. M. Nichols, *EMD and instantaneous phase detection of structural damage*, in Hilbert–Huang Transform and Its Applications: World Scientific, 2014, pp. 301-336.

[12] M. A. Neto, A. Amaro, L. Roseiro, J. Cirne, and R. Leal, *Engineering computation of structures: the finite element method*. Springer, 2015.